Fusion Engineering and Design 22 (1993) 415–426
North-Holland

Chemical compatibility of SiC composite structures with fusion reactor helium coolant at high temperatures

F.J. Perez * and N.M. Ghoniem

Mechanical, Aerospace and Nuclear Engineering Department, School of Engineering and Applied Science, University of California, Los Angeles, CA 90024, USA

Submitted 29 June 1992, accepted 23 November 1992
Handling Editor: Robert W. Conn

The thermodynamic stability of SiC/SiC composite structures proposed for fusion applications is presented in this paper. Minimization of the free energy for reacting species in the temperature range 773–1273 K is achieved by utilizing the NASA-Lewis Chemical Equilibrium Thermodynamics Code (CET). The chemical stability of the matrix (SiC), as well as several fiber coatings (BN and graphite) are studied. Helium coolant is assumed to contain O_2 and water moisture impurities in the range 100–1000 ppm. The work is applied to recent Magnetic and Inertial Confinement Conceptual designs. The present study indicates that the upper useful temperature limit for SiC/SiC composites, from the standpoint of high-temperature corrosion, will be in the neighborhood of 1273 K. Up to this temperature, corrosion of SiC is shown to be negligible. The main mechanism of weight loss will be by evaporation to the plasma side. The presence of a protective SiO_2 condensed phase is discussed, and is shown to result in further reduction of high-temperature corrosion. The thermodynamic stability of C and BN is shown to be very poor under typical fusion reactor conditions. Further development of chemically stable interface materials is required.

1. Introduction

Silicon carbide ceramic matrix composites are proposed candidate low-activation materials for structural components in fusion reactors because of their high strength, adequate thermal conductivity and good thermal shock resistance. In this application, the material is inevitably exposed to either oxidizing or reducing gases; therefore, a thorough understanding of the gaseous corrosion behavior of the material at elevated temperatures is important.

When SiC is exposed to a strongly oxidizing atmosphere, such as air, a dense SiO_2 layer forms on the surface, and further oxidation is retarded. Because of this passivation, SiC exhibits excellent oxidation resistance at high temperatures. However, when the supply of oxygen is not sufficient (in reducing or inert atmospheres), the protective SiO_2 layer cannot form, and weight loss occurs by decomposition or active oxidation of the SiC. Such corrosion can significantly affect the strength of the SiC by introducing flaws in the surface or reducing the load-bearing cross section.

It is important to state that the chemical stability of SiC/SiC, SiC/C and SiC/BN at high temperatures is undetermined at present. The main objective of the present work is to study the degradation behavior of these materials under typical fusion reactor conditions.

The main coolants considered for fusion reactors are: Helium, CO_2, Li and Li–Pb. The present work focuses on helium coolants containing oxygen or water moisture impurities. It is practically and thermodynamically impossible to eliminate such impurities. The residual oxidizing impurities are very important in obtaining and maintaining a good SiO_2 protective layer. Under fusion conditions, the temperature of the SiC structure which is in contact with the coolant can vary between 773 and 1273 K, and the impurity content of the helium coolant between 10 and 1000 parts per million (ppm). These conditions represent a typical environment for high-temperature corrosion processes. The growth of a surface oxide can be compared with

* Permanent address: Departmento de Ciencia de los Materiales, Facultad Ciencias Qumimicas, Universidad Complutense, Madrid-28040. And Instituto de fusion Nuclear, ETSI Industriales, Universidad Politecnica, Madrid-28006.

the current flow around a circuit containing an electrolytic cell, including both electronic and ionic parts. The ionic current produces two effects:

(a) ionization of metal atoms: $Me = M^{z+} + Ze^-$

(b) ionization of oxygen atoms: $O + 2e^- = O^{2-}$

These are anodic and cathodic processes, respectively. The metal ions are attracted towards cathodic surfaces, while the oxygen atoms are attracted towards anodic surfaces. During the growth of a solid non-porous oxide, either species may be immobile, but the other one will be mobile. An oxide film grows by ionic transport, but there must also be electron movement. Electrons move in the same direction as the positively charged metal ions or in the reverse direction to the negatively charged oxygen ions. Electron movement through oxides is associated with defects in the oxide lattice. Ionic diffusion is determined by the movement of ions between vacant lattices sites and is much slower than the movement of electrons.

In a neutron and gamma radiation environment, as is the case in fusion reactor structural materials, further ionization and creation of vacancies are expected. High temperature corrosion rates can therefore be enhanced by the radiation flux. We will not consider this aspect of corrosion in the present work.

2. Thermodynamic analysis

The computer code CET, developed by NASA-Lewis Research Center, is used in the present study to calculate the equilibrium composition of reacting chemical species. This procedure is based on the minimization of the total free energy of the system, which was originally developed by Gordon and McBride, and revised by Zeleznick [1]. The total Gibbs free energy of a system is given by:

$$G = \sum_{i=1}^{n} n_i g_i = \sum_{i=1}^{n} n_i \left(g_i^0 + RT \ln a_i \right) \tag{1}$$

Table 1
Conditions for chemical compatibility study

Material	Impurities	Assumed range
SiC	H_2O	100–1000 ppm.
	O_2	100–1000 ppm.
BN	H_2O	100–1000 ppm.
	O_2	100–1000 ppm.
C	H_2O	100–1000 ppm.
	O_2	100–1000 ppm.

where G is the total Gibbs free energy of a system, R the ideal gas constant, T the thermodynamic temperature, N_i the moles of chemical species i, and a_i the activity of species i. When ideal conditions are assumed in each phase, equation (1) becomes:

$$\frac{G}{RT} = \sum_{p=1}^{n} \sum_{i=1}^{m_p} n_{pi} \left[\left(\frac{g^0}{RT} \right)_{pi} + \ln P + \ln \left(\frac{n_{pi}}{N_p} \right) \right] + \sum_{p=2}^{q+1} \sum_{i=1}^{m_p} n_{pi} \left[\left(\frac{g^o}{RT} \right)_{pi} + \ln \left(\frac{n_{pi}}{N_p} \right) \right] + \sum_{p=q+2}^{q+s+1} \sum_{i=1}^{m_p} n_{pi} \left(\frac{g^o}{RT} \right)_{pi} \tag{2}$$

where n_{pi} is the moles of species i in phase p, N_p the total moles of species in phase p, m_p the number of species in phase p, and P the total pressure. In equation (2), $p = 1$ corresponds to the gaseous phase. The mass of all elements must be conserved:

$$\sum_{p=1}^{q+s+1} \sum_{i=1}^{m_p} C_{pij} n_{pi} = b_j \ (j = 1, 2, \cdots), \tag{3}$$

where C_{pij} is the number of atoms of element j and i the total number of elements. The set of n_{pi}, which minimize equation (2) is the equilibrium composition of the system. To calculate n_{pi} in eq. (2), the free energy of each reaction, must be known and can be expressed by:

$$\frac{g^0}{RT} = \left(\frac{1}{R} \right) \left[\frac{(G^0 - H_{298}^0)}{T} \right] + \Delta_f \frac{H_{298}^0}{RT}. \tag{4}$$

Thermodynamic data are included with the program for 62 reactants and 421 reaction species (solid, liquid, and gas phases of all species are counted as separate species). The data are mostly obtained from JANAF tables, although additional elements and reactions can be included [26,27].

The reference conditions are that of a recent ICF Fusion reactor study (Prometheus [2]) and a magnetic confinement reactor study (Aries [3,4]), both with helium coolant. These conditions are summarized in table 1. The average temperature range for the study is between 773 and 1273 K.

3. Chemical reactions

Silicon carbide will chemically react with O_2, H_2O and H_2, according to the following reactions:

$$SiC(s) + O_2(g) \rightleftharpoons SiO(g) + CO(g), \quad (5)$$

$$2SiC(s) + 3O_2(g) \rightleftharpoons SiO(g) + CO_2(g), \quad (6)$$

$$2SiC(s) + O_2(g) \rightleftharpoons SiO(g) + C(s), \quad (7)$$

$$SiC(s) + O_2(g) \rightleftharpoons Si + CO_2(g), \quad (8)$$

$$2SiC(s) + O_2(g) \rightleftharpoons Si + CO(g), \quad (9)$$

$$SiC(s) + 2H_2O(v) \rightleftharpoons SiO(g) + CO(g) + 2H_2(g), \quad (10)$$

$$SiO_2(s)(\text{protective layer}) + H_2(g) \rightleftharpoons SiO(g) + H_2O(v). \quad (11)$$

Relevant reactions for forming a solid protective layer are given below. Formation of the solid oxide layer will be a function of the partial pressure of oxygen in the system:

$$SiC(s) + 2O_2(g) \rightleftharpoons SiO_2(s) + CO_2(g), \quad (12)$$

$$2SiC(s) + 3O_2(g) \rightleftharpoons SiO_2(s) + CO(g), \quad (13)$$

$$SiC(s) + O_2(g) \rightleftharpoons SiO_2(s) + C(s). \quad (14)$$

For the C and BN fibers, the following relevant reactions are considered:

$$C(s) + O_2(g) \rightleftharpoons CO_2(g), \quad (15)$$

$$2C(s) + O_2(g) \rightleftharpoons 2CO(g), \quad (16)$$

$$2BN(s) + 2O_2(g) \rightleftharpoons 2BO_2(g) + N_2(g), \quad (17)$$

$$2BN(s) + 3H_2O(v) \rightleftharpoons B_2O_3(g) + 2NH_3(g), \quad (18)$$

$$4BN(s) + 3O_2(g) \rightleftharpoons 2B_2O_3(g) + 2N_2(g), \quad (19)$$

$$2BN(s) + O_2(g) \rightleftharpoons B_2O_2(g) + N_2(g), \quad (20)$$

$$3BN(s) + 3H_2O(v) \rightleftharpoons 2NH_3(g) + N_2(g) + 3BO(g), \quad (21)$$

$$2BN(s) + 6H_2O(v) \rightleftharpoons 2H_3BO_3(g) + 2NH_3(g), \quad (22)$$

$$BN(s) + 2H_2O(v) \rightleftharpoons HBO_2(g) + NH_3(g). \quad (23)$$

The kinetics of the last reactions can be affected by the formation of a protective layer of SiO_2 at high oxygen partial pressures such that SiC is stable in many corrosive environments. Figure 1 shows, in arbitrary corrosion units, a schematic of the protective layer. It is interesting to note that when the coolant contains higher oxide impurity levels, SiC will tend to form a protective oxide coating, which would prevent further oxidation.

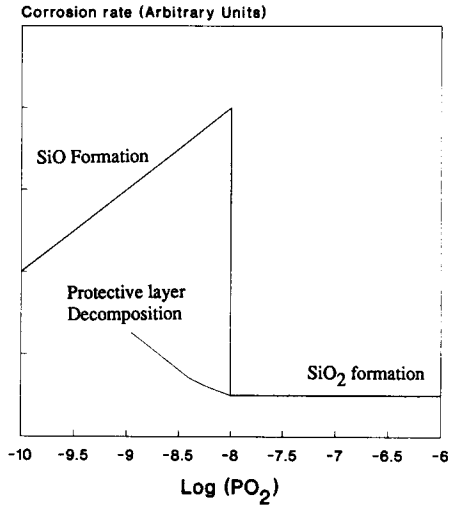

Fig. 1. Stability schematic in SiO_2 in fusion coditions.

4. Results of chemical equilibrium thermodynamic analysis

As mentioned previously, H_2 and H_2O will be present in some quantities in certain sections of the reactor blanket. Water will result from the reaction of H_2 with residual O_2, while H_2 will be present as an additive to the carrier gas in the breeding blanket, as well as from (n,p) reactions and the plasma in the first wall materials. Studies of the stability of SiC in H_2 environments have been conducted primarily for applications in the National Aerospace Plane and in the Ceramic Stirling Engine, where H_2 chemical activities are considerably greater than expected in a Fusion Blankets [5,6]. In the following, we give results of computations for SiC/SiC composites, for an SiC/C interface, and for an SiC/BN interface.

4.1. SiC / SiC composites

The thermodynamic stability of SiC in pure H_2 at 1 atmosphere is shown in fig. 2, the primary gaseous product is methane (CH_4), while other reactions that produce SiH_4 and SiH are also possible at temperatures relevant to fusion conditions. The effects of methane formation on the behavior of SiC structures must be carefully studied, since hydrogen isotopes will

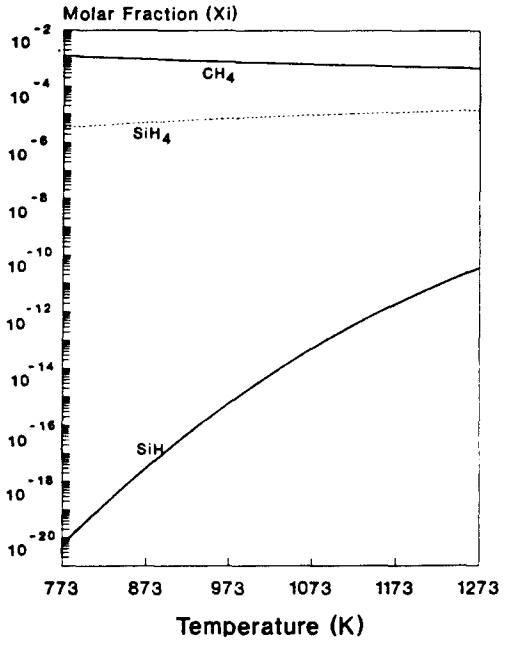

Fig. 2. Molar fraction for gases in equilibrium with SiC in pure H_2 at 1 atmosphere.

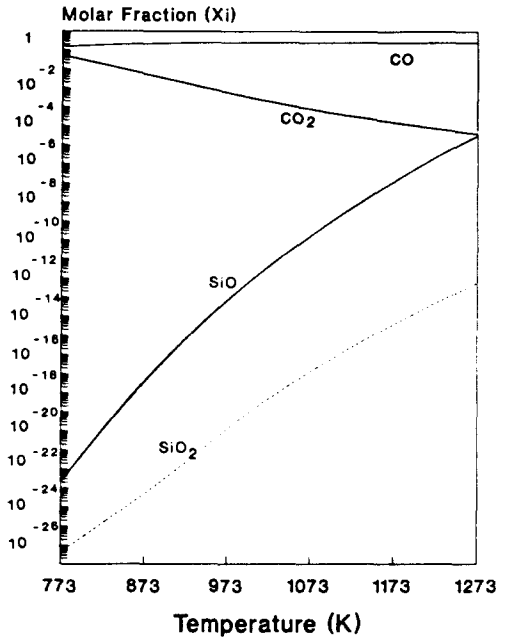

Fig. 3. Molar fraction for gases in equilibrium with SiC in contact with 100 ppm O_2 in helium coolant.

be produced in SiC. In the plasma chamber first wall and diverter, the helium coolant and the tritium recovery systems are different, and the concentration of hydrogen in the two streams can be quite different. The tritium recovery system will contain higher levels of H_2 available to react with the SiC. The tritium recovery system will contain a high content of hydrogen isotopes, and will be dependent on design details. However, this aspect of H_2 reactions with SiC is separately treated in section 4.1, and the equilibrium concentrations are given in fig. 2. We will illustrate these features again in section 8. Since the current work deals only with the subject of high-temperature corrosion, we did not attempt to assess the effects of possible high concentrations of methane (CH_4), and other gaseous products (e.g. SiH_4 and SiH) on the operation and design of the tritium recovery system.

Figure 3 shows the molar fractions of gases in equilibrium with SiC in contact with a helium coolant containing 100 ppm. O_2. The primary gaseous products formed are CO and CO_2, with small quantities of SiO and SiO_2. These volatile species exist in equilibrium with the condensed phase of SiO_2 (protective layer in these conditions).

The molar fractions of condensed phases are shown in fig. 4. It can be immediately seen that the formation

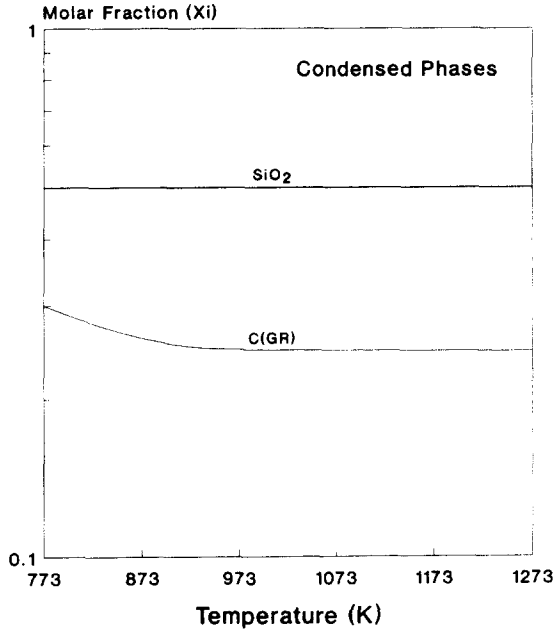

Fig. 4. Molar fraction of condensed species in equilibrium with SiC. Helium coolant with 100 ppm O_2.

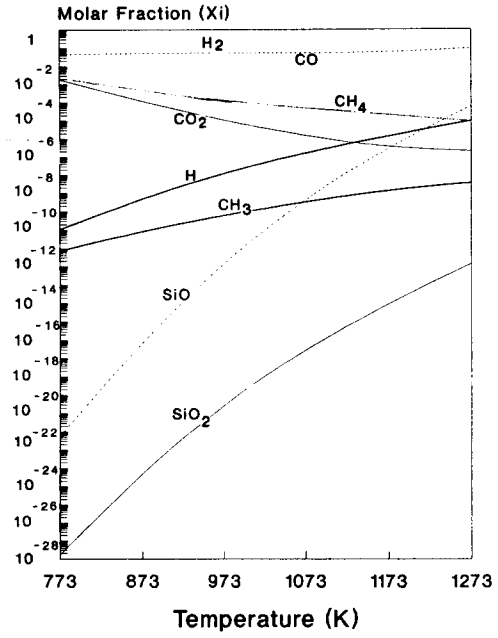

Fig. 5. Molar fraction gases in equilibrium with SiC. Helium coolant with 100 ppm H_2O.

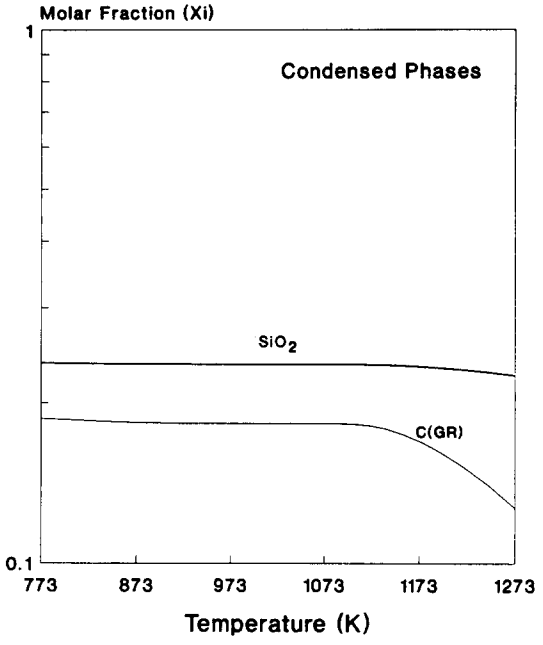

Fig. 6. Molar fraction of condensed phases in equilibrium with SiC. Helium coolant with 100 ppm H_2O.

of the protective layer of SiO_2 is thermodynamically favorable over the temperature range of interest. The growth of this layer is parabolic with time, as is conventional with solid state oxidation.

Figure 5 shows the molar fractions of gases in equilibrium with SiC, when the helium coolant contains 100 ppm H_2O, as typical levels of impurities in helium. It is observed from these figures that the production of volatile gaseous species is higher than the previous case. The high concentration of hydrocarbons would result in etching the C-side of SiC. The break-down of water molecules, and their subsequent chemical reactions with Si and C results in higher oxidation levels of carbon atoms, as compared to silicon. As a consequence, the more aggressive environment of water moisture is associated with a smaller molar fraction of the protective oxide layer, as seen in fig. 6.

4.2. Thermodynamic stability of graphite fiber–matrix interfaces

One of the commonly used interfaces for SiC/SiC composites is graphite. This interface controls fiber pull-out which influences toughness. It is important,

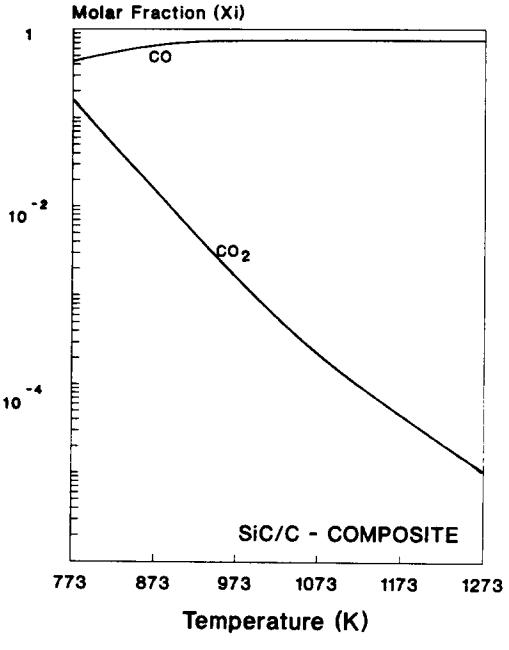

Fig. 7. Molar fraction of gases in equilibrium with C. Helium coolant with 100 ppm O_2.

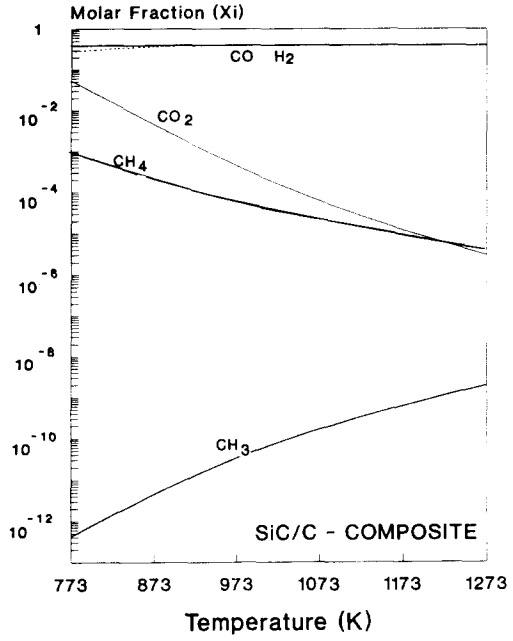

Fig. 8. Molar fraction of gases in equilibrium with C. Helium coolant with 100 ppm H_2O.

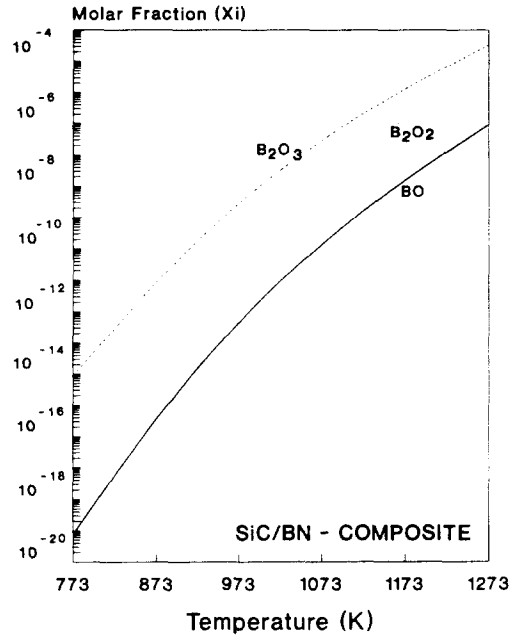

Fig. 9. Molar fraction of gases in equilibrium with BN. Helium coolant with 100 ppm O_2.

however, to investigate the thermodynamic stability of carbon interfaces.

The molar fractions of volatile gases in equilibrium with C are shown in fig. 7, for helium coolant containing oxygen impurities at the level of 100 and 1000 ppm, respectively. When the results are compared with SiC (fig. 3), it is seen that the molar fractions of CO are far greater than the corresponding values for the SiC system. When water moisture exists in the helium coolant, the decomposition of graphite is even worse. Figure 8 shows the main gaseous species for 100 ppm H_2 impurity level.

4.3. Thermodynamic stability of boron nitride fiber–matrix interface

Molar fractions of volatile gaseous species in equilibrium with BN interface are shown for oxygen impurities (fig. 9); and for water impurities, fig. 10. The main problem in this case is the effect of hydrogen on the stability of BN. Oxygen impurities alone do not result in decomposition of BN. However, when hydrogen is present, the decomposition is complete, as can be observed in fig. 11.

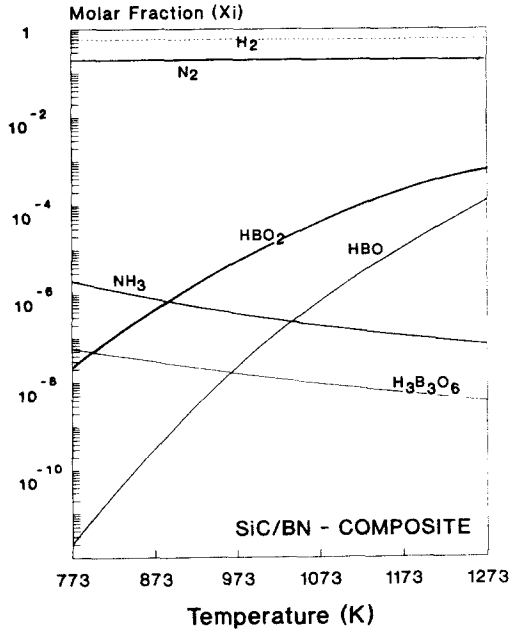

Fig. 10. Molar fraction of gases in equilibrium with BN. Helium coolant with 100 ppm H_2O.

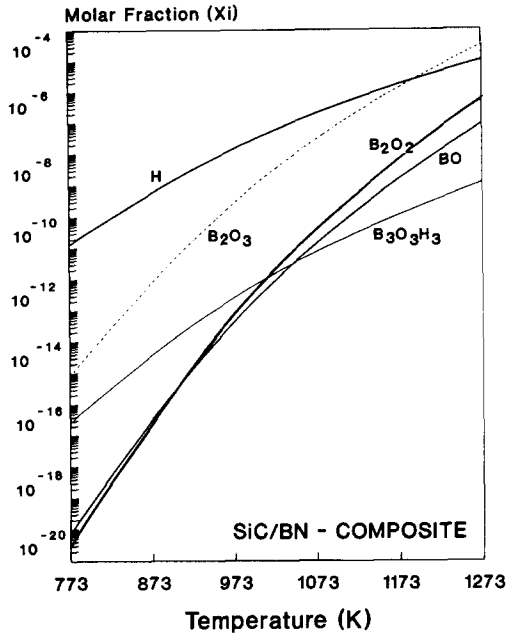

Fig. 11. Molar fraction of gases in equilibrium with BN. Helium coolant with 100 ppm H_2O.

5. Oxidation mechanisms of silicon carbide

The oxidation of SiC at reaction interfaces generates very low oxygen partial pressures. If active oxidation does not occur, the silica formed at the reaction interface is expected to be oxygen deficient with the formation of corresponding defects: vacancies, 3-bonded silicon and possibly Si pairs. Vacancy formation is particularly important for fusion applications. Under the intense neutron flux of a fusion reactor, displacement damage will generate higher concentrations of vacancies, and hence is expected to enhance the high-temperature corrosion of SiC.

Two types of contributions are possible for the transport of oxygen in SiC, the first mechanism is molecular, in which molecules of oxygen are transported through channels in vitreous silica. The second is a network contribution, which can occur through the various network defects. Assuming that the major model of network transport is by a vacancy mechanism, the equation for the total diffusion coefficient is given by:

$$D = D_v C_v + D_m C_m. \tag{24}$$

D_v and D_m are the vacancy and molecular diffusion coefficients, and C_v and C_m are the vacancy and molecular concentrations, respectively. Therefore the kinetics of silica oxidation will depend on the relative contribution of the two transport paths, which is determined by stoichiometry at a given temperature. Under low oxygen pressures, the quantity of dissolved oxygen (C_m) and the concentration of oxygen vacancies (C_v) will be increased, tending to favor transport by a vacancy mechanism over transport by molecular diffusion [7,8].

The two sides of a single crystal SiC, under oxidizing fusion conditions, maintain their stoichiometric character as they oxide. The two elements of SiC qualitatively maintain their relative rates of oxidation during the early oxidation for thicknesses of silica up to 20Å, even after surface mixing due to sputtering. This carbonization of the carbon side explains the evolution of silicon under the very low oxygen pressure at the site of the reaction [9]:

$$2SiC + O_2 \rightleftharpoons 2CO + Si. \tag{25}$$

Under one atmosphere of oxygen, it is assumed that this difference in stability of the two elements is maintained, and that silicon still tends to be volatile from the C-side. However, both carbon and oxygen are oxidized in the reaction:

$$SiC + O_2 \rightleftharpoons SiO + CO. \tag{26}$$

As shown in fig. 12, it is possible by this reaction to always maintain the order of the Si and C atoms at the interface, so that on the C-side it is always at the surface of the SiC as it oxidizes, thus maintaining the C-side behavior. The SiO oxidizes as it meets with the higher oxygen pressure near the interface. The silica forms as a rough porous scale, and a rough interface results from the active oxidation reaction. As further oxidation proceeds, SiO oxidizes in the pores, so that

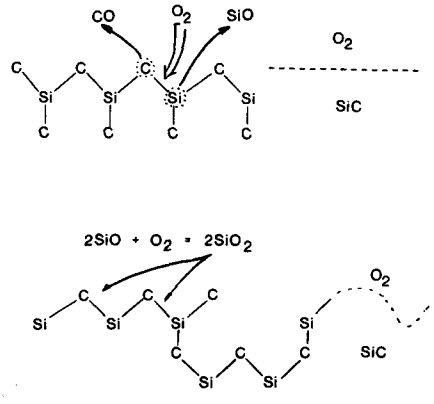

Fig. 12. Model for oxidation of C-side of SiC.

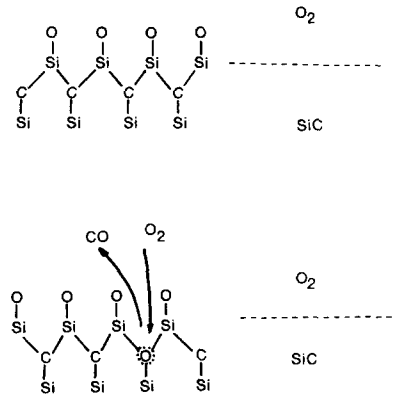

Fig. 13. Model for oxidation of SiC-side of SiC.

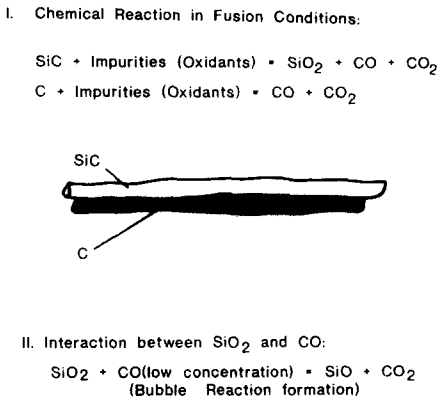

Fig. 14. Mechanism of corrosion of SiC/C composite.

scale porosity is filled. The scale if formed under higher partial pressures found at the interface, and will therefore not be stoichiometric.

On the Si-side, however, silicon atoms are segregated at the surface. It is proposed that oxygen is absorbed first on the silicon layer (fig. 13), and the carbon is then oxidized by penetration of oxygen through this oxide layer, maintaining silicon between the oxide and SiC. The scale formed under these conditions would be more oxygen deficient than that formed at the Si-side. In the oxidation of SiC, both network and molecular transport mechanisms add to supply the oxygen. This interplay between the two types of transport processes continues as the temperature is increased, and their relative contribution changes for the Si-side and C-side. As the temperature is increased, transport by vacancy and other network mechanisms with high activation energies increases rapidly and becomes a major contributor to the oxidation of the carbon side. The oxidation of SiC therefore increases, since it is dominated by network transport processes. As the temperature is increased, atomic mobility is increased at the SiC interfaces, and oxidation can no longer be differentiated by the mechanisms proposed. Therefore, the proposed model is qualitatively consistent with the data on the oxidation of SiC [10].

6. Synergistic degradation mechanisms of SiC / C composites

Figures 14 and 15 show a proposed mechanism for the oxidation of SiC/C system, where the interface Si-C is the point of localized corrosion in the fibers. In this case, the system can not form a continuous protective layer of SiO_2. Figure 13 shows the first step of the chemical reactions for the formation of the protective layer:

$$SiC + \text{impurities (oxidants)} \rightleftharpoons SiO_2 + CO + CO_2. \quad (27)$$

Under these conditions the carbon fiber will react according to:

$$C + \text{impurities (oxidants)} \rightleftharpoons CO + CO_2. \quad (28)$$

In this case, we will have interaction between SiO_2 and CO, as follows:

$$SiO_2 + CO \text{ (low concentration)} \rightleftharpoons SiO + CO_2. \quad (29)$$

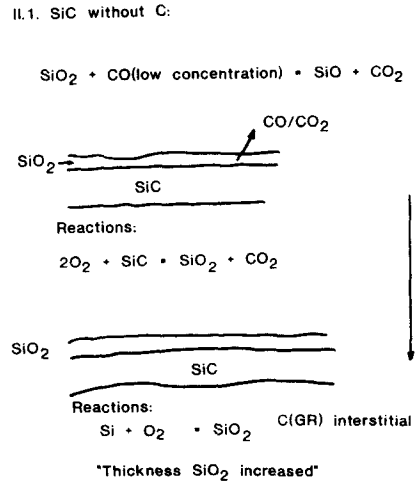

Fig. 15. Mechanism of corrosion of SiC/C composite.

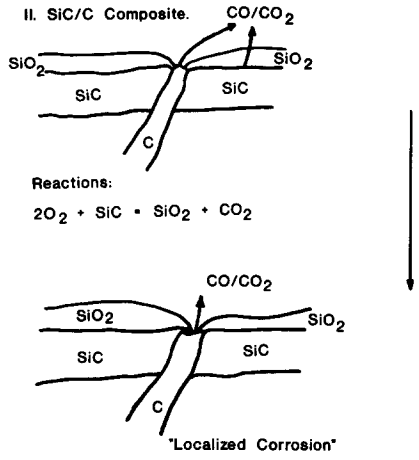

Fig. 16. Mechanism of corrosion of SiC/C composite.

The last reaction is very important to consider at the interface between SiO_2 and C because it not only destroys the protective layer on the SiC, but it also forms CO_2 gas bubbles. Figure 14 illustrates this mechanism on SiC only, where the formation of CO_2 and CO is important only in the first step of the reaction. After this carbon step, the formation of CO_2 decreases with time, and SiC forms the protective layer under fusion conditions.

Figure 15 illustrates the degradation mechanism in the SiC/C system. In this case, the formation of CO and CO_2 is very localized at the Si–C interface, because of the continuous formation of bubbles in the system. CO_2 reacts with SiO_2 and forms gaseous SiO, and localized corrosion takes place at the Si/C interface (Fig. 16). The protection of the solid phase of SiO_2 is lost in this case.

7. Gas phase diffusion through cracks

Composites invariably contain micro-cracks, which may be caused by an expansion coefficient mismatch between the matrix and the fiber. For example, if the matrix has a higher expansion coefficient than the fiber and the composite is processed at high temperature, the matrix will be stressed upon cooling to room temperature and micro-cracks form by residual stresses.

The effects of oxygen diffusion through the cracks depend on the matrix and the substrate. If the matrix is an oxidizable material, such as SiC, which getters oxygen, oxygen diffusion through the cracks will react with the matrix and may possibly seal the crack. However, if the matrix is an oxide, which cannot getter any oxygen, oxygen will diffuse rapidly through the cracks. In this situation, the oxidation rate of the substrate will depend upon the nature of the oxidation product and its interaction with the matrix oxide.

8. Maximum corrosion rates in fusion reactor conditions

At low pressures, where the molecular mean free path is longer than the system size, the number of molecules leaving or striking a unit surface area per second, ϕ, is given by:

$$\phi = \tfrac{1}{4} V_m n. \tag{30}$$

The last equation can be easily derived from the kinetic theory of gases. Here, n, is the number of molecules per unit volume, and V_m is the mean molecular velocity. If the mass of each molecule is m, the equilibrium mass evaporation rate can be calculated as:

$$W = \tfrac{1}{4} n m V_m = \tfrac{1}{4} \rho V_m, \tag{31}$$

where ρ is the gas density. The mean velocity V_m is given by:

$$V_m = \sqrt{\frac{8RT}{\pi M}}, \tag{32}$$

where R is the gas constant, T the absolute temperature and M the molecular weight. Combining the two last equations, we get:

Equation (34) gives us the corrosion rate in kg cm^{-2} s^{-1}, that we have transformed to micrometers per year.

$$W(\text{kg cm}^{-2}\text{ s}^{-1}) = \frac{1MP}{4RT}\sqrt{\frac{8RT}{2\pi RT}}, \tag{33}$$

$$W(\text{kg cm}^{-2}\text{ s}^{-1}) = P\sqrt{\frac{M}{2\pi RT}}. \tag{34}$$

The kinetic model, expressed in eqs. (33) and (34) is applied to the evaluation of the evaporation corrosion rate of silicon carbide in two recent conceptual fusion reactor studies: Prometheus [2] and Aries-I [3,4]. The evaporation of the first wall material into the plasma side in the Aries-I concept is analyzed at a temperature of 1323 K. The corrosion rate in first wall at the coolant side (helium with impurities) is also computed.

Figure 17 shows that the evaporation corrosion rate of SiC in typical fusion conditions, increases with temperature. This evaporation rate will be compared later

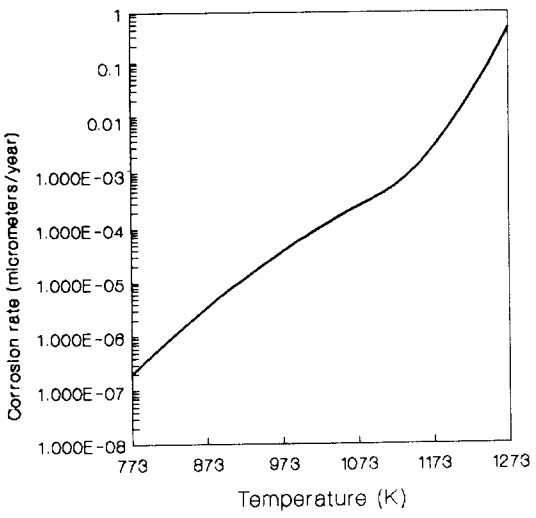

Fig. 17. Evaporation corrosion rate of SiC. Fusion conditions.

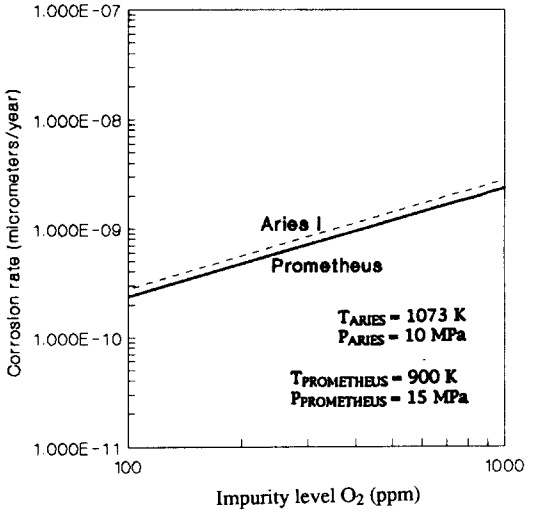

Fig. 19. Hot corrosion in Prometheus and Aries I.

with the corrosion rate in Prometheus and Aries due to coolant impurities. It is found that at all temperatures, the evaporation corrosion rate is higher than the corrosion rate due to coolant impurities. Both reactor designs show good resistance to high temperature corrosion.

Figure 18 shows results of computations for helium coolant with 100 ppm H_2O. A comparison between the corrosion rate due to evaporation and that due to the corrosion process in the coolant. It is shown that in the Aries design, the difference between the corrosion rate due to evaporation and that due to hot corrosion is smaller than that with Prometheus design. Figures 19 and 20 show a comparison of the maximum corrosion rate due to hot corrosion for both the Prometheus and Aries design concepts, with various impurity levels. It can be seen that the corrosion rate is higher for the Aries design for both O_2 and H_2O impurities. However, the corrosion rate for both reactors is higher

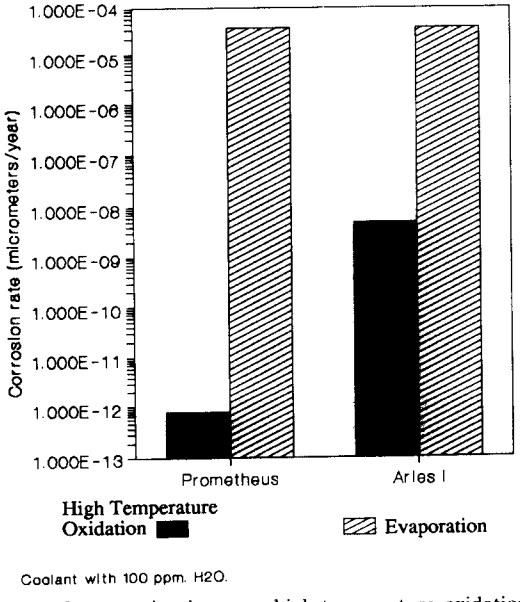

Fig. 18. Comparation between high temperature oxidation of SiC and the evaporation corrosion rate in both reactors.

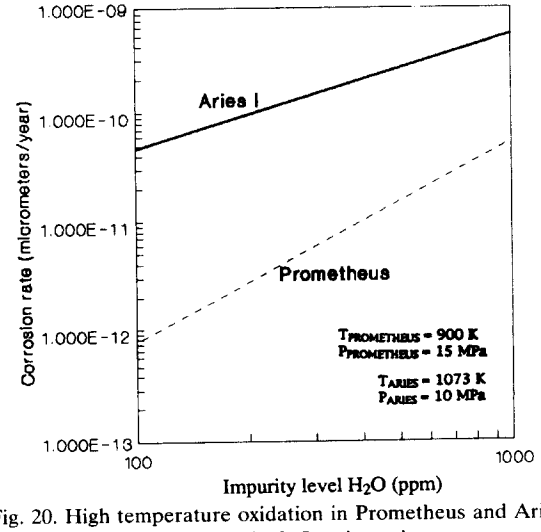

Fig. 20. High temperature oxidation in Prometheus and Aries I. Coolant with H_2O as impurity.

when the coolant contains O_2 impurities as compared to H_2O. So, for the same average impurity levels, the material will form the SiO_2 protective layer, and the corrosion rate is lower with H_2 impurities.

9. Conclusions

SiC/SiC composite structural materials are shown to have attractive high-temperature corrosion resistance characteristics, in addition to their low neutron activation and high temperature structural capabilities. The present study shows the following conclusions:

(1) The presence of hydrogen and hydrogen isotopes from nuclear reactions, and from solid breeder will result in the formation of hydrocarbons, primarily methane (CH_4). The equilibrium molar fraction of methane is approximately 0.01, over a wide range temperatures. Therefore, it is expected that methane gas will exist in the first wall and blanket regions.

(2) Typical oxygen and water impurities result in the formation of a self-healing, and stable SiO_2 oxide layer, which prevent further oxidation.

(3) The chemical stability of SiC/SiC composites with either graphite or BN interfaces is not assured with these interface materials. Other types of chemically-stable interface may have to be developed, or the access of oxygen to fibers be limited.

(4) Typical fusion reactor designs, both magnetic (Aries) and Inertial (Prometheus), show that the hot corrosion rates in the first wall and blanket systems will be very negligible.

(5) Evaporation of SiC into the plasma side will dominate over chemical hot corrosion. Nevertheless, both rates are practically insignificant.

References

[1] S. Gordon, B.J. McBride and J. Zeleznick, Computer program for calculation of complex chemical equilibrium composition, NASA-Lewis Research Center, NASA TM-86885 (October, 1984).

[2] M.S. Tillack, M.Z. Youssef, M.A. Abdou, A.R. Raffray, J. Eggleston, A. El-Azab, Z. Gorbis, F. Issacci, I. Jun, S. Sharafat, A.Y. Ying and N. Ghoniem, Initial design of the Prometheus wetted wall IFE reactor cavity, UCLA-FNT-51 (October, 1991).

[3] S. Sharafat for the Aries Group, Applications of SiC composites in Aries, Proceedings of the Office of Fusion Energy/DOE Workshop on Ceramic Matrix Composite for Structural Applications in Fusion Reactors, Santa Barbara, May, 1990.

[4] R.W. Conn et al., The Aries-I tokamak reactor study: Final report, UCLA-PPG-1323, Vols. I and II (1992).

[5] S. Morozumu, Joining of silicon carbide, J. Nucl. Mater. 169 (1989) 270–272.

[6] D.C. Larsen et al., Ceramic materials for advances heat engines, Noyes Rep. (1985) pp. 234–236.

[7] J.R. Blanchere and F.S. Petit, High temperature corrosion of ceramics, Noyes Data Corp. (1989).

[8] G. Ervin, Jr., Oxidation behavior of silicon carbide, Journal of American Ceramic Society 41, No. 9 (YEAR?) 347–353.

[9] J.R. Blanchere and F.S. Petit, High temperature corrosion of ceramics, DOE Report ER 10915-4 (June, 1984).

[10] T. Narushima, T. Goto and T. Hirai, High temperature passive oxidation of chemically vapor deposited carbide, Journal of American Ceramic Society 72, No. 8 (1989) 1386–1390.

[11] Z. Zheng, R.E. Tresler and K.E. Spear, Oxidation of single crystal silicon carbide: Part I. Experimental studies, Journal of Electrochemical Society 137, No. 3 (1990) 854–8.

[12] K. Luthra and H.D. Park, Oxidation of silicon carbide reinforced oxide-matrix composites at 1375 to 1575°C, J. of American Ceramic Society 73, NO. 8 (1990) 10124–1023.

[13] N.S. Jacobson, A.J. Eckel, A.K. Misra and D.L. Humphrey, Reactions of SiC with H_2, H_2O, argon mixtures at 1300°C, J. of American Ceramic Society 73, No. 8 (1990) 2330–2332.

[14] K.L. Luthra and D.H. Park, Oxidation issues in C/oxide composites, 13th Annual Conference of Composites and Advanced Ceramics, January 15–18, 1989, Florida.

[15] B.E. Deal and A.S. Grove, General relationship for thermal oxidation of silicon, J. of Appl. Phys. 36, No. 12 (1986) 3770–3778.

[16] L.U. Ogbuji, Development of oxide scale micro structures on single-crystal SiC, J. of Mater. Sci. 16 (1981) 2753–2759.

[17] S.C. Singhai, Oxidation kinetics of hot-pressed silicon carbide, J. of Mater. Sc. 11 (1976) 1246–1253.

[18] A. Heuer and V.L.K. Lou, Volatility diagrams for silica, silicon nitride and silicon carbide and their application to high temperature decomposition and oxidation, J. of American Ceramic Society 73, No. 10 (1990) 2785–3128.

[19] R. Warren and C.H. Anderson, Silicon carbide fibers and their potential for use in composite materials, Part II, Composites 15, No. 2 (1984) 101–111.

[20] G. Morscher, P. Pirouz and H. Heuer, Temperature dependence of interfacial shear strength in SiC-fiber-reinforced reaction-bounded silicon nitride, J. of American Ceramic Society 73, No. 3 (1990) 713–720.

[21] G.L. Kulcinski et al., An investigation into the use of graphite and silicon carbide in ion beam reactors, University of Wisconsin Report, UWFDM-426 (1989).

[22] S.G. Seshadri and M. Srinivasan, Liquid corrosion and

high-temperature oxidation effects on silicon carbide/titanium diboride composites, J. of American Ceramic Society 71 No. 2 (1988) C72–C74.

[23] D.J. Pysher, C. Goretta, R.S. Hodder, Jr. and R.E. Tressler, Strengths of ceramic fibers at elevated temperatures, J. of American Ceramic Soc., No. (4) (1989) 284–288.

[24] W.L. Vaughn and H.G. Maashs, Active-to-passive transition in the oxidation of silicon carbide and silicon nitride in air, J. of American Ceramic Society 73, No. 6 (1990) 1540–1543.

[25] N.S. Jacobson and J.L. Smialek, Corrosion pitting of SiC by molton salts, J. of Electrochemistry Society 133, No. 12, (1986) 2615–2624.

[26] N. Ghoniem, Thermodynamic stability and high temperature corrosion of rhenium in rocket nozzle exhaust cones, Final Project Report, Ultramet Inc. (September, 1990).

[27] A.J. Sherman, R.H. Tuffias, A.S.R. Chew and N. Ghoniem, Modeling of the Compatibility of rhenium with solid rocket motor exhaust, Proceedings of the 1990 JANAF Propulsion Meeting, CPIA, Vol. 55, 1991, October 2–4, 1990, Anaheim, CA.

[28] H.E. Kim and A.J. Moorhead, Effect of hydrogen-water atmospheres on corrosion and flexural strength of sintered SiC, J. of American Ceramic Society 73, No. 8 (1990) 694–699.

[29] N.S. Jacobsen, A.J. Eckel, A.D. Misra and D.L. Humphrey, Reactions of SiC with $H_2/H_2O/Ar$ mixtures at 1300°C, J. of American Ceramic Society 73 (91990) 2330–2334.

[30] S. Morozumi, Joining of SiC, J. Nucl. Mater. 69 (1989) 270–272.

[31] M. Maeda, K. Nakamura and M. Yamada, Oxidation resistance evaluation of SiC ceramics with various additives, J. of American Ceramic Society 72, No. 3 (1989) 512–514.